cAMP-Coupled Riboflavin Trafficking in Placental Trophoblasts: A Dynamic and Ordered Process†

Vanessa M. D'Souza,‡,§ Amy B. Foraker,‡,§ R. Benjamin Free,|| Abhijit Ray,‡ Paul S. Shapiro,‡ and Peter W. Swaan*,‡

Department of Pharmaceutical Sciences, University of Maryland, Baltimore, Maryland 21201, and Molecular Neuropharmacology Section, National Institute of Neurological Disorders and Stroke, National Institutes of Health, Bethesda, Maryland 20852-9405

Received January 21, 2006; Revised Manuscript Received March 21, 2006

ABSTRACT: Riboflavin (RF, vitamin B_2), an essential micronutrient central to cellular metabolism through formation of flavin mononucleotide (FMN) and flavin adenine dinucleotide (FAD) cofactors, is internalized, at least in part, via a proposed receptor-mediated endocytic (RME) process. The purpose of this study was to delineate the cellular RF distribution using human placental trophoblasts and evaluate the regulatory role of cAMP in this process. Subcellular fractionation and three-dimensional confocal microscopy analyses were carried out to define the RF accumulation profile. Biochemical assays evaluating the cAMP dependence of this pathway were also performed. This study records an intracellular RF distribution pattern that shows dynamic accumulation of the ligand predominantly in the endosomal and lysosomal compartments and to a lesser extent in the Golgi and mitochondria. In contrast, transferrin (TF) colocalizes rapidly within endosomes with minimal accumulation in the other organelles. The temporal and spatial distribution of RF and TF colocalized with unique markers of the endocytic machinery provides added morphological evidence in support of the RME process with ultimate translocation to the mitochondrial domain. Colocalized staining with the Golgi also suggests a possible recycling or exocytic mechanism for this ligand. Furthermore, this study demonstrates cAMP regulation of the putative ligand-bound RF receptor and its association into endocytic vesicles. Delineating the dynamics of the process governing cellular RF homeostasis presents an untapped resource that can be further exploited in improving our current understanding of nutritional biology and fetal growth and development, and perhaps in targeting the endogenous system for developing novel therapeutic approaches.

Dietary intake of free riboflavin (vitamin B_2, RF)[1] or release from the coenzyme forms, flavin mononucleotide (FMN) and flavin adenine dinucleotide (FAD), determines the nutritional status of this essential nutrient in humans. Physiological deficiency of RF accounts for clinical manifestations of growth retardation, anemia, cardiovascular disease, and neurodegenerative disorders (*1*, *2*). Despite the critical role of flavin analogues in normal cellular metabolic processes, little is known about the mechanism and regulation of the vitamin B_2 absorptive process. Investigative approaches based on biochemical characterization and two-dimensional fluorescence microscopy have identified a putative receptor-mediated component to be responsible, at least in part, for RF uptake in human enterocytes and trophoblasts. High ligand binding affinity (nanomolar range), temperature and ion dependence, and a saturable process that can be inhibited by structurally related ligands are the salient features that describe this system (*3*−*5*). Analogous to iron recruitment and absorption, the proposed RF entry mechanism involves initial recognition by specific binding proteins that chaperone the hydrophilic ligand across membrane barriers within vesicles (*6*). However, the identity of these proteins and other components that facilitate the absorption of this essential nutrient remains elusive. Consequently, elucidating the driving mechanisms that contribute to the cellular homeostasis of this vitamin has generated considerable interest from the standpoint of nutritional biology and fetal growth and development, with potential application in targeted drug design and delivery (*7*, *8*).

Internalization of extracellular nutrients in eukaryotes via receptor-mediated endocytosis employs complex cell machinery in a sequential and regulated manner. The coexistence of abundant intracellular structural and signaling networks offers several possibilities for receptor-associated ligands. Most water-soluble vitamins are fated to metabolic

† This study was supported by funds from the National Institutes of Health Grant DK56631 (to P.W.S.) and the Susan G. Komen Breast Cancer Foundation (PDF0402815).

* To whom correspondence should be addressed: Department of Pharmaceutical Sciences, University of Maryland, 20 Penn St., Baltimore, MD 21201. Telephone: (410) 706-0103. Fax: (410) 706-5017. E-mail: pswaan@rx.umaryland.edu.

‡ University of Maryland.

§ These two authors contributed equally to this work and should be considered as co-first authors of this paper.

|| National Institutes of Health.

[1] Abbreviations: cAMP, cyclic adenosine 5′-monophosphate; CTMR4A, carboxytetramethylrhodamine-4-amine; DIC, differential interference contrast; FAD, flavin adenine dinucleotide; FITC−TF, fluorescein isothiocyanate-labeled transferrin; FMN, flavin mononucleotide; LAMP1, lysosome-associated membrane protein; Rd−RF, rhodamine−riboflavin; RF, riboflavin; RME, receptor-mediated endocytosis; TCA, taurocholic acid; TF, transferrin.

10.1021/bi060138f CCC: $33.50
Published on Web 04/15/2006

trapping, a term that describes enzymatic processing of the molecule to forms that are spatially restricted within the cell (*9*). However, alternative translocation routes, including late endosomal or lysosomal degradation, membrane recycling, or even transcytosis (in polarized epithelial systems), remain a distinct possibility (*10*). Such receptor−ligand interactions also occur under extensive cellular regulation either via an intrinsic mechanism such as kinase or phosphatase activity or via generation of signaling cascades that include second-messenger regulation of integrated pathways (*11*, *12*). Huang and colleagues (*4*) have demonstrated that the RF internalization process is affected by modulation of the cyclic nucleotide second messengers, cAMP and cGMP, as well as by protein kinase A, protein kinase G, and calcium−calmodulin pathways.

The objective of this study was to evaluate the fate of internalized RF over time by following its intracellular sorting using the human placental trophoblast cell line, BeWo (*13*), and to define the regulatory role of cyclic AMP in this process. The enhanced nutritional requirements of the fetus (*14*−*17*) and the presence of a high-affinity RF system (*4*) justify the use of the selected model that was compared with another human polarized epithelial system, Caco-2 cells with nanomolar affinity for RF (*3*). Time- and concentration-dependent fractionation analyses of the localized ligand in endosomes, lysosomes, Golgi, and mitochondria were compared with confocal laser scanning microscopy studies examining time-lapse three-dimensional (3D) colocalization between internalized rhodamine-labeled RF (Rd−RF) (*18*, *19*) and immunolabeled organelles. Trafficking profiles for RF were compared with those determined for transferrin (TF), a receptor-mediated endocytic marker (*20*−*22*), and for taurocholic acid (TCA) that does not follow a vesicular pathway (*23*, *24*). In addition, cyclic AMP assays were included to determine regulation of the downstream events of cellular RF translocation upon its binding to the proposed RF receptor. Overall, the study for the first time shows that RF, like TF, accumulates mainly within endosomes but differs from TF in the extent of lysosomal distribution. This study also suggests a possible recycling mechanism that contributes to RF homeostasis and regulation via the cAMP signaling pathway in the trophoblast model.

EXPERIMENTAL PROCEDURES

Cell Culture. The BeWo and Caco-2 cells were obtained from American Type Culture Collection (Manassas, VA) and routinely maintained in a controlled atmosphere at 37 °C, under 5% CO_2. BeWo (passage numbers 206−221) and Caco-2 (passage numbers 30−48) cells were routinely cultured in F-12K and DMEM medium, respectively (Invitrogen Life Technologies, Carlsbad, CA) supplemented with 10% fetal bovine serum, 1% nonessential amino acids, 100 units/mL penicillin, and 100 μg/mL streptomycin. Cells were seeded in 150 mm culture dishes at a density of 3×10^4 cells/cm^2 and were used 5−7 days postseeding for fractionation studies.

Labeling of Transferrin. Holotransferrin was labeled with Na^{125}I (~5 μCi/μg; Amersham Biosciences, Piscataway, NJ) using the IODOGEN method (Pierce Biotechnology, Inc., Rockford, IL). Iodinated protein was desalted by gel filtration using Micro-Bio-Spin columns (Bio-Rad Laboratories, Hercules, CA), and the extent of ^{125}I incorporation was determined by gel electrophoresis and autoradiography. The specific activity of the [^{125}I]transferrin was ~ 400 cpm/pmol.

Ligand Uptake and Subcellular Fractionation. Cell monolayers were treated with 10 nM [^{3}H]riboflavin (Sigma, St. Louis, MO) and 10 nM [^{125}I]transferrin in Hanks' Balanced Salt Solution (HBSS, pH 7.4) containing 25 mM glucose and 10 mM HEPES at 37 °C for 2 h. After incubation, cells were washed thoroughly with ice-cold Dulbecco's phosphate-buffered saline (DPBS) containing Ca^{2+} and Mg^{2+} (pH 3.0) to remove plasma membrane-associated ligands. Cells were then pooled in homogenization buffer containing 0.25 M sucrose, 10 mM Tris-HCl (pH 7.5), and protease inhibitors (Complete Mini, Roche) and allowed to swell for 15 min prior to being lysed through a 25G$^{5/8}$ hypodermic needle monitored by phase-contrast microscopy. The cell homogenate was centrifuged at 600*g* for 5 min at 4 °C to yield a nuclear pellet (N) and postnuclear supernatant (PoN). The total protein content of each fraction was measured using the Bradford assay (Bio-Rad Laboratories).

Endosomes, lysosomes, Golgi, and mitochondria were isolated by loading the PoN fraction on a discontinuous sucrose gradient (from 0.8 to 2.0 M) and subjected to centrifugation at 205000*g* for 2 h at 4 °C using a SW 55Ti rotor (Beckmann Coulter, Inc., Fullerton, CA). The gradient was top-fractionated into 350 μL aliquots. Accumulation of radiolabeled ligands in each fraction was assessed by a quench-curve corrected dual-label (i.e., ^{3}H and ^{125}I) liquid scintillation counting program (Beckmann Coulter, Inc.) and normalized to the total protein content determined by the Bradford assay. Time- and concentration-dependent enrichment of riboflavin and transferrin to these organelles were assessed by varying incubation times (from 30 min to 2 h) and ligand concentrations (from 5 to 25 nM), respectively. Each experiment was run in replicate, but because of the variability associated with the top fractionation method, the profiles do not exactly coincide between runs. Hence, as is typically shown, the fractionation data are a representative image for the ligand distribution profiles.

Immunoblotting and Data Analysis. Cellular organelles in the collected fractions were identified by Western blot analyses using monoclonal antibodies (BD Pharmingen, San Diego, CA) directed against organelle-specific protein markers (i.e., Rab5 GTPase and clathrin for early endosomes, LAMP-1 for lysosomes, GM130 for Golgi, and cytochrome *c* for mitochondria). Fractionated proteins were resolved on 7.5 or 18% Tris-HCl gels, transferred to PVDF membranes (Immun-Blot, Bio-Rad), immunoblotted using peroxidase-conjugated secondary antibodies, and detected using the ECL plus system (Amersham Biosciences). Sequentially fractionated samples that were positive for a specific protein marker were grouped together to represent that particular organelle population. The subcellular ligand distribution to the individual organelle population was expressed as a percentage of the total ligand content in the PoN fraction. Due to overlap of marker expression between fractions, the ligand distribution exceeds 100% but serves as a semiquantitative approach for identifying the ligand trafficking pathway(s) upon internalization.

Immunofluorescence and Confocal Microscopy. Cells were seeded 3−5 days prior (5×10^3 cells/cm^2) in collagen-coated BD Falcon culture slides (BD Biosciences, Bedford, MA).

Following serum starvation, pulse−chase studies with either 500 nM rhodamine−RF (*18*) or 30 nM FITC−transferrin conjugate (FITC−TF, Sigma) were carried out as previously described (*19*). Cells were then fixed, permeabilized, and blocked prior to immunolabeling for 2 h at room temperature to detect organelle markers (clathrin, Rab5 GTPase, LAMP-1, GM130, or cytochrome *c*). Cells were washed thoroughly and probed with either AlexaFluor546- or AlexaFluor405-labeled sheep anti-mouse IgG (Molecular Probes, Eugene, OR). Immunofluorescence treatments were preserved using GelMount (Biomeda Corp., Foster City, CA) and visualized using a Nikon Eclipse TE2000 E inverted confocal laser scanning microscope equipped with three fixed lasers, 488, 405, and 543 nm (average of two scans per channel). All 3D confocal images were acquired using the following parameters on Nikon EZ-C1 acquisition software (Gold version 2.3, Image Systems, Inc., Columbia, MD): Nikon Plan Apo 60xA oil objective (1.4 numerical aperture), 6.00 μs scan dwell time, 512 × 512 pixel size, 0.25 μm *z*-step, 60 or 150 μm detector pinhole, and constant attenuation of a 488 nm laser using a neutral density filter (ND8). Images were iteratively deconvolved using a calculated point spread function for each fluorescent channel and corrected using intensity thresholds defined by treatment with either rhodamine or secondary antibodies alone, and by applying a median filter. All images were then analyzed to define 3D colocalized regions using Volocity, version 3.6 . The extent of colocalization between fluorescent ligands and AlexaFluor-labeled organelles was determined by calculating the percent of total overlapping volume between the two channels compared to the corresponding total ligand volume. All data were averaged using three to four regions of colocalized distributions, and statistical significance was determined using Pearson's correlation (*25*).

Determination of the Extent of Cyclic AMP Accumulation in BeWo Cells. BeWo cells were seeded for assays aimed at evaluating the cAMP response to the RF stimulus (2.5×10^5 cells/well) and cAMP inhibition assays (1.0×10^5 cells/well), 1 day prior to use in 24-well Biocoat plates (BD Biosciences). Cells were washed with Earle's Balanced Salt Solution (EBSS, pH 7.4) and incubated at 37 °C with 10^{-12} to 10^{-3} M stimulant for the indicated times in 250 μL of stimulation buffer [20 mM HEPES-buffered F12K (pH 7.4) containing 30 μM Ro-20-1724, a phosphodiesterase inhibitor, and 200 μM sodium metabisulfite, an antioxidant]. Negative coupling assays were carried out by preincubating cells with varying RF concentrations for 10 min prior to stimulation of cells with 1 μM forskolin. The reaction was terminated by discarding the stimulation buffer and adding 200 μL of 3% perchloric acid per well. After incubation on ice for 30 min, 80 μL of 15% $KHCO_3$ was added to each well, and the plates were further incubated for 10 min. The plates were then centrifuged for 10 min at 1300*g*. Subsequently, 50 μL of the supernatant from each well was transferred to 250 μL of reaction mixture (150 μL of Tris-EDTA buffer, 50 μL of cAMP-binding protein, and 50 μL of [^{3}H]cAMP) and incubated at 4 °C overnight. On the following day, 250 μL of charcoal/dextran mix (1%) was added to each sample followed by incubation at 4 °C for 15 min and then centrifugation for 15 min at 1300*g*. Radioactivity in the supernatant from each tube was quantified by liquid scintillation counting. Cyclic AMP concentrations were calculated using a standard curve according to the protocol of the assay kit (Diagnostic Products Corp., Los Angeles, CA).

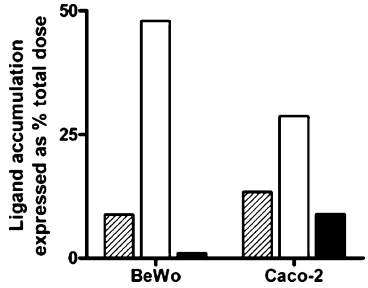

FIGURE 1: Comparative cell-associated profiles of [^{3}H]riboflavin (10 nM RF) with the endocytic marker [^{125}I]transferrin (10 nM TF) and an unrelated bile acid transporter substrate, [^{3}H]taurocholic acid (20 nM TCA), in placental (BeWo) and intestinal (Caco-2) cells. Ligand content derived from nuclear and postnuclear fractions and expressed as the percent of total dose revealed ≥8% RF accumulation (hashed bars), while TF levels (white bars) varied from 48% in BeWo cells to 28% in Caco-2 cells. The distribution profile of TCA (black bars) showed negligible accumulation in trophoblasts vs enterocytes.

RESULTS

Isolation of Organelle-Enriched Fractions. Cell homogenates following ligand exposure were centrifuged to separate the denser membrane fragments and nuclei from the lower-density organelles. Separation of nuclei was confirmed by DAPI staining (Molecular Probes). Another polarized epithelial system, the human intestinal Caco-2 cell line, which also exhibits nanomolar affinity for RF (*3*), was used in parallel. The total intracellular content of riboflavin that accumulated within the fractionated compartments was compared with that of transferrin and taurocholic acid, taken to be positive and negative controls for the receptor-mediated endocytic process, respectively. As expected, the BeWo- and Caco-2-associated profiles for TF when expressed as the percent of total dose revealed substantial ligand accumulation (28−48%) independent of cell line. Likewise, the riboflavin load in the fractions was ≥8%, but TCA exhibited poor accumulation, at least in BeWo cells (Figure 1). Such distinct distribution profiles for RF, TF, and TCA in cells from different tissue origins provide validation of the isolation procedure. However, the reduced level of accumulation of the negative marker for endocytosis (TCA) and prior evidence of a higher-affinity RF transport system (nearly 10-fold difference) in the BeWo cell line justifies its selection over the Caco-2 model for subsequent ligand distribution analyses.

The protein content of the nuclear fractions was significantly higher (∼5 times) than that for postnuclear fractions that had protein yields varying between 2.3 and 4.95 mg/mL. However, the protein load per gradient was kept constant. The identity of the fractionated gradient was determined by Western blot analyses for organelle-specific markers. Clathrin heavy chain (180 kDa), a protein component of the endocytic vesicle coat (*26*), and Rab5 GTPase (25 kDa), a GTP-binding protein, associated with early endosomes (*27*), were detected mainly in fractions 1−7 isolated from BeWo cells (Figure 2B,C). Likewise, Caco-2 cells upon subcellular fraction analysis showed a similar distribution of clathrin, but Rab5 GTPase was restricted to fractions 1 and 2 (data not shown). Lysosome-associated

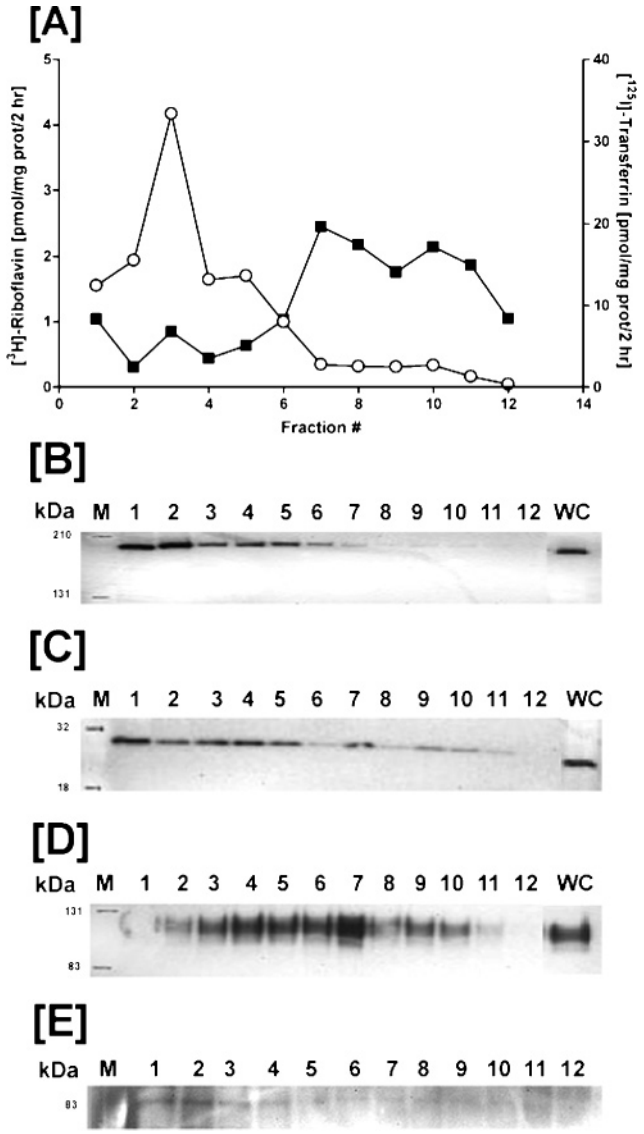

FIGURE 2: Distribution of [^{3}H]riboflavin (RF) and [^{125}I]transferrin (TF) in the postnuclear fractions isolated from trophoblasts. (A) Postnuclear fractions isolated from BeWo cells were resolved on the basis of differential organelle densities using a discontinuous sucrose gradient, fractionated, and measured for dual radiolabel accumulation: (■) [^{3}H]RF and (○) [^{125}I]TF. Organelle-enriched fractions were identified by Western blot analyses using antibodies directed against endosomal proteins, namely, clathrin (B) and Rab5 GTPase (C), and the lysosomal marker LAMP-1 (D). (E) Intact radiolabel on TF following homogenization and gradient fractionation was visualized at ~83 kDa by gel electrophoresis and autoradiographic exposure of the isolated fractions.

membrane protein (LAMP-1, 110 kDa) (*28*) indicated the presence of lysosomes in fractions 3−10 (Figure 2D). Due to overlap in protein markers between fractions, the organelles were not exclusive to any given fraction; instead, pooled fractions were considered enriched for a defined subcellular population.

Distribution of Internalized RF and TF. To evaluate the intracellular localization profile of RF after cellular entry, BeWo cells were loaded for 2 h at 37 °C with RF and TF. The endocytic uptake and processing of TF enabling cellular iron transfer have been well-documented (*20*), thereby supporting its use as a marker with which to contrast the trafficking pattern(s) of RF. Following incubation with the ligands, subcellular fractions isolated from trophoblasts by

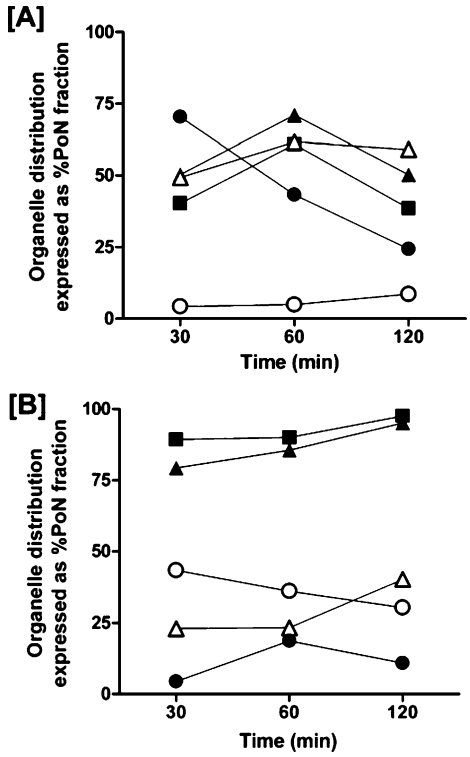

FIGURE 3: Time-dependent localization of [^{3}H]RF and [^{125}I]TF within the separated fractions from BeWo cells. Sucrose density gradient fraction analysis by Western blotting of organelle-associated markers [(■) clathrin, (▲) Rab5 GTPase, (△) LAMP-1, (○) GM130, and (●) cytochrome *c*] following exposure to RF (A) and TF (B) for 30, 60, and 120 min revealed ligand-specific distribution profiles.

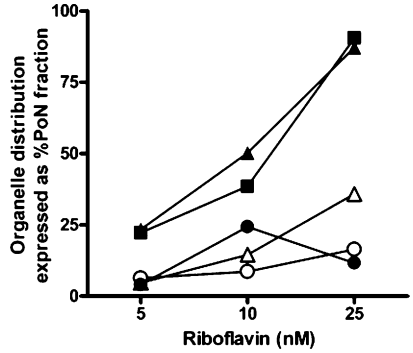

FIGURE 4: Concentration-dependent trafficking profiles of [^{3}H]RF after incubation for 2 h at 37 °C. The level of ligand accumulation of 5−25 nM RF in endosomes [(■) clathrin and (▲) Rab5 GTPase], lysosomes [(△) LAMP-1], Golgi [(○) GM130], and mitochondria [(●) cytochrome *c*] increased in a dose-dependent manner in placental trophoblasts.

density gradient centrifugation were measured for radiolabeled RF and TF by liquid scintillation counting. Subcellular distribution patterns for [^{3}H]RF and [^{125}I]TF measured in the postnuclear organelle fractions from placental cells resulted in localized bands of the radiolabels along the sucrose gradient. RF was detected mainly in the heavier fractions (fractions 7−12), whereas TF appeared to concentrate in the less dense fractions (fractions 2−7) of the gradient (Figure 2A). Degradation of [^{125}I]TF resulting in loss of label during the cell homogenization and fractionation process poses a potential concern. Hence, the integrity of the marker following processing was verified by autoradiography, which revealed intact protein at ~83 kDa in all fractions containing

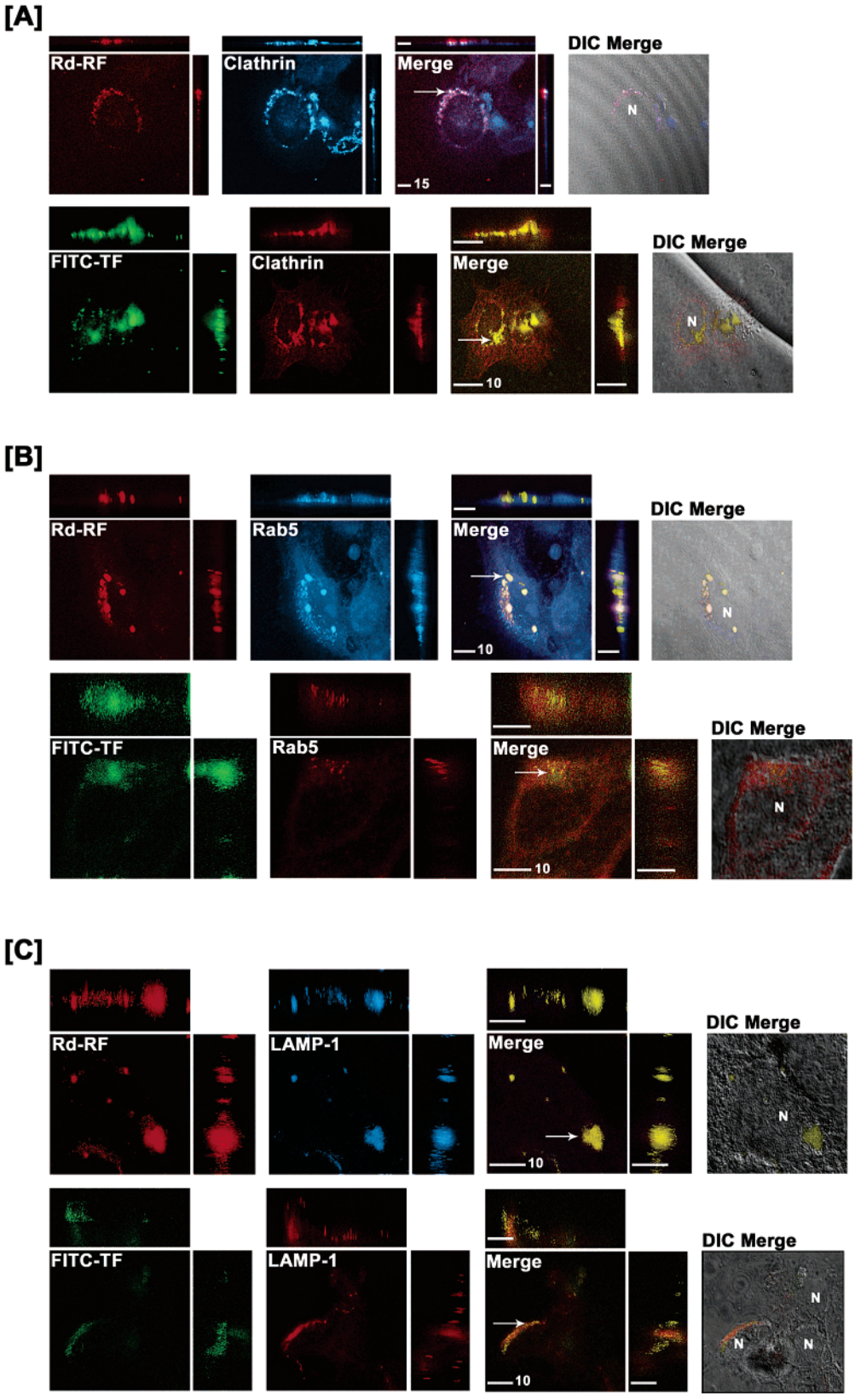

FIGURE 5: Endosomal and lysosomal colocalization of rhodamine−RF (Rd−RF) and FITC-labeled transferrin (FITC−TF). Rd−RF or FITC−TF were examined for colocalization with immunostained early endocytic [clathrin (A) and Rab5 GTPase (B)] and lysosomal [LAMP-1 (C)] protein markers after ligand internalization in BeWo cells for 60 min. Images represent orthogonal 3D profiles with the inset view defining the $X-Y$ plane, and the outer panels reveal the $Y-Z$ (right narrow panel) and $X-Z$ (top narrow panel) focal planes. Fluorescence signals for each channel were merged to reveal regions of colocalization (indicated by arrows and yellow regions) and overlaid with the corresponding differential interference contrast (DIC) image to define cell morphology (far right inset view). Both Rd−RF and FITC−TF exhibited distinct colocalization with early endosome markers for clathrin and Rab5 GTPase. In contrast to FITC−TF, Rd−RF exhibited an extensive colocalized signal with LAMP-1. The nucleus is represented by N. Scale bars (micrometers) are defined in the merged inset views.

transferrin (Figure 2E). Consequently, the organelle isolation process did not interfere with the compartmentalization and detection of TF.

Labeling of BeWo cells with 10 nM RF and 10 nM TF resulted in a differential rate of ligand buildup. At the end of 2 h, RF exhibited a slower rate of internalization [i.e., 22.1−33.6 pmol (mg of protein)$^{-1}$ h^{-1}] than TF that accounted for almost one-third to one-half of the administered dose [i.e., 71.5−119.7 pmol (mg of protein)$^{-1}$ h^{-1}]. Quantitative ligand distribution at 2 h associated with the organelle-enriched fractions as determined from marker protein evaluation showed ∼38−50% of postnuclear RF content in the endosomes in BeWo cells (Figure 3A), whereas endosomal fractions from Caco-2 cells accounted for ∼7−13% of the same ligand (data not shown). Like RF, TF also exhibited increased signal intensities in the endosomal regions (≥95%) in BeWo cells at 2 h (Figure 3B), which is in accordance with previous reports showing TF accumulation within an acidic nonlysosomal compartment (*29*−*31*). Although the extent of lysosomal accumulation of TF in Caco-2 cells was significantly lower than the endosomal levels, RF was distributed in equivalent amounts between the two endocytic organelles (data not shown).

Ligand-specific differences were detected in their time-dependent endosomal and lysosomal accrual. In BeWo cells, RF localization in endosomes (∼45%) and lysosomes (∼10%) within 30 min occurs less rapidly than TF endocytosis (Figure 3A,B). The level of endosomal and lysosomal accumulation of RF reached a maximum at the end of 1 h (Figure 3A) and declined by 30−35% after 2 h. In contrast, the endosomal and lysosomal content of TF in BeWo cells increased over time with maximal deposition in the endosomes at 2 h (Figure 3B). Caco-2 cells, on the other hand, demonstrate a more rapid RF internalization process with maximum vesicular localization at 30 min that declines over 2 h (data not shown). Conversely, the level of TF cargo within the endosomal fractions of Caco-2 cells increases while lysosomal levels decrease over the 2 h period (data not shown). Differences in ligand accumulation profiles over time suggest differential requirements for vitamin B_2 or iron that are met via multiple and simultaneous mechanisms in a cell-specific manner. Furthermore, evaluation of the concentration-dependent accumulation of RF (5−25 nM) in BeWo cells revealed a dose-dependent increase in the vesicular buildup of the ligand (Figure 4), thus confirming active uptake via the endocytic machinery.

Colocalization of RF with Endocytic Organelles. The cellular distribution of internalized RF was further examined using a characterized rhodamine-labeled riboflavin conjugate (Rd−RF) that exhibits affinity characteristics similar to those of the natural vitamin (*19*). Since maximal accrual of RF within endocytic organelles in BeWo cells occurred after 60 min, all fluorescence-based studies were performed using this uptake period. Internalized Rd−RF or FITC−TF was examined for colocalized signals with AlexaFluor405- or AlexaFluor546-labeled proteins for endosomes (clathrin or Rab5) and lysosomes (LAMP-1) using confocal laser scanning microscopy. Signal intensities specific to Rd−RF were normalized to cells treated with equimolar amounts of a nonreactive rhodamine analogue, carboxytetramethylrhodamine-4-amine (CTMR4A) (*18*). In all cases, the signal-to-noise ratio for CTMR4A was significantly lower than that

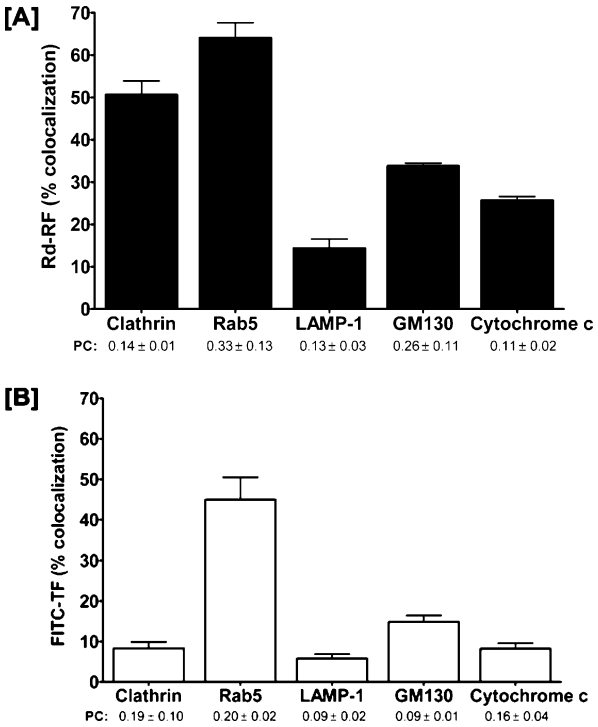

FIGURE 6: Quantitative evaluation of the 3D colocalized regions of RF and TF with organelle protein markers. Overlapping, i.e., colocalized, volumes (cubic centimeters) for either Rd−RF (A) or FITC−TF (B) with organelle channels were expressed as a percentage of the total volume for Rd−RF or FITC−TF. Pearson's correlation (PC) was chosen to define the similarity of 3D shapes between ligands and overlapping channels with organelle markers. Data are expressed as the mean ± the standard error of the mean for three to four regions of interest. All values were greater than 0.0 and, thus, revealed a positive correlation for pattern recognition between channels.

for Rd−RF, and in contrast to those of Rd−RF, staining patterns were routinely diffuse (data not shown). Like FITC−TF, internalized Rd−RF resulted in distinct punctate, perinuclear staining and colocalization with both clathrin and Rab5 GTPase (Figure 5A,B). In contrast to FITC−TF, Rd−RF also exhibited partial colocalization with the lysosomal marker, LAMP-1 (Figure 5C).

A quantitative assessment of the extent of colocalization between ligands and endocytic markers revealed maximal signal overlap with Rab5 GTPase for both Rd−RF (64%) and FITC−TF (45%) (Figure 6A,B). Compared to the 60 min fractionation data in Figure 3, the total RF distribution to this endosome population (∼70%) is strikingly similar to that seen with Rd−RF. However, the extent of FITC−TF colocalization with Rab5-positive endosomes was nearly 2-fold lower compared to that defined in the fractionation results. This disparity may be attributed to the presence of a heterogeneous subpopulation of endosomes that are Rab5-negative but TF-positive, an incidence that cannot be detected by subcellular fractionation due to the fractional overlap. Rd−RF also revealed ∼51% colocalization with clathrin, whereas FITC−TF exhibited only 8% overlapping signal with this early endosome protein. The Pearson's correlation (PC), a common statistical test for shape similarities exhibited between colocalized fluorescent channels, was used to further define linear relationships existing between ligands and organelle markers. Values >0.0 were defined as having a positive linear relationship between variables (*25*). Interest-

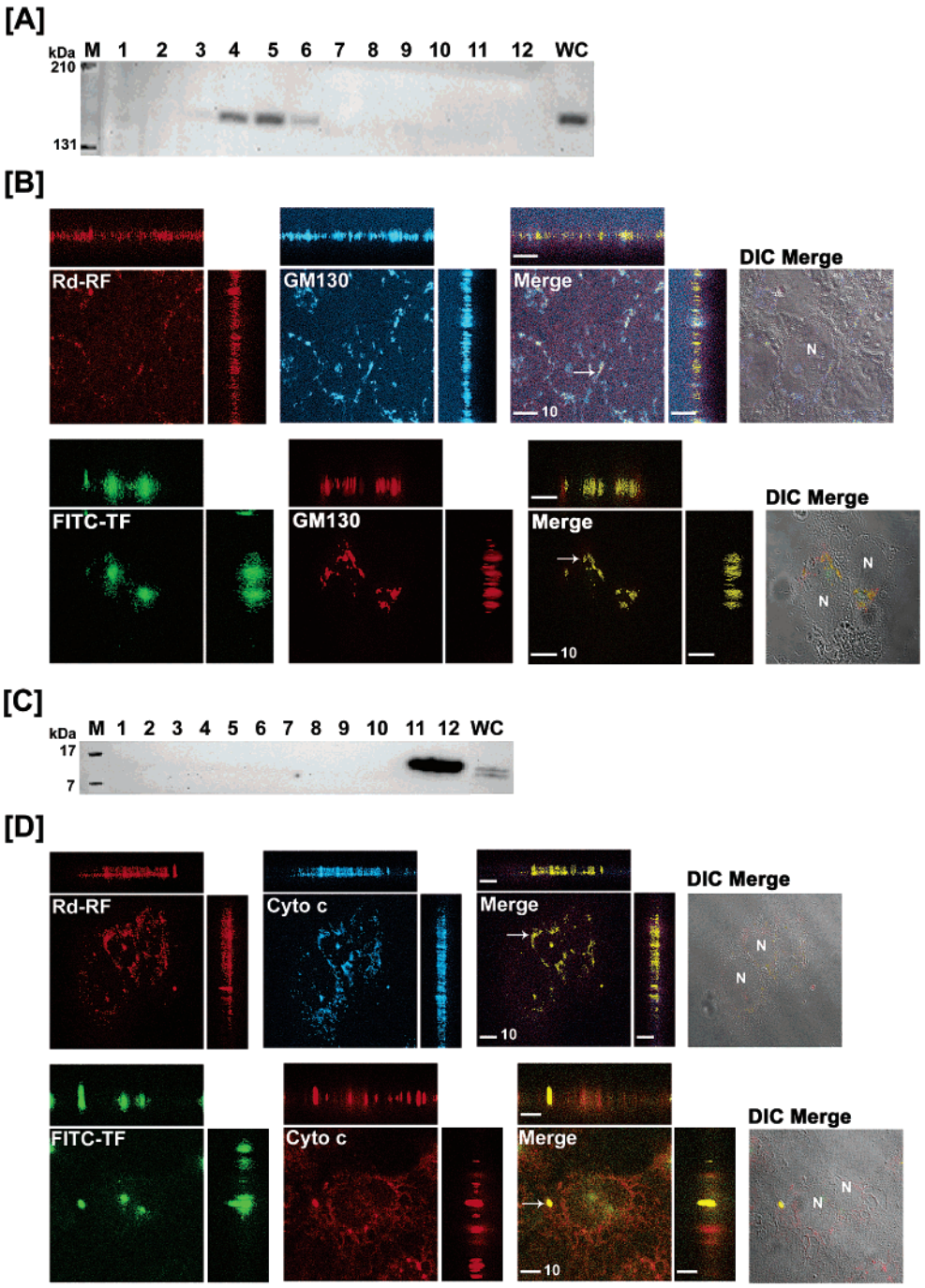

FIGURE 7: Translocation of [^{3}H]RF and [^{125}I]TF to the Golgi and mitochondria in BeWo cells. Postnuclear fractions collected after internalization of [^{3}H]RF and [^{125}I]TF in BeWo cells for 2 h were immunoblotted for Golgi [GM130 (A)] and mitochondria [cytochrome *c* (C)]. Confocal 3D images of either Rd−RF or FITC−TF after internalization in BeWo cells for 60 min were analyzed for colocalization (arrows and yellow regions) with Golgi (B) and mitochondria (D). Confocal images are defined by orthogonal profiles as described in the legend of Figure 5, and fluorescent signals were merged with DIC images (right columns in panels B and D). Scale bars represent 10 μm, and nuclei (N) are defined in DIC images.

ingly, both ligands revealed positive correlations with all organelle-associated proteins (Figure 6). Consistent for both Rd−RF and FITC−TF, the relative levels of colocalization (14 and 6%, respectively) with the lysosome protein, LAMP-1 (Figure 6), were markedly lower than those determined for each ligand enriched to endosomes. Although both ligands revealed colocalization with LAMP-1, the overall enrichment with lysosomes is suggested to be minimal. Collectively, these results indicate significant ligand recruitment for both RF and TF to early or sorting endosomes via plasma membrane-associated clathrin and/or Rab5-positive vesicles (*27*, *32*, *33*). In contrast to TF, the internalized RF demonstrates greater lysosomal accumulation. RF that bypasses lysosomal degradation is likely to be sorted to recycling endosomes, similar to apotransferrin which undergoes exocytosis at the plasma membrane (*34*).

Golgi and Mitochondrial Involvement in the RF Itinerary. Intracellular enrichment of RF to the Golgi and mitochondria in comparison with that for TF was also examined in the isolated subcellular fractions. GM130 (130 kDa), a structural marker of the Golgi apparatus (*35*) was identified in postnuclear fractions 4−6 (Figure 7A), while nuclear frac-

tions 11 and 12 tested positive for cytochrome *c* (15 kDa), an integral component of the mitochondrial respiratory chain (*36*) (Figure 7C). The steady-state distribution (2 h) showed 6−8% of RF (Figure 3A) and 30−37% of TF (Figure 3B) distributed to the Golgi. Interestingly, mitochondrial localization of RF in BeWo cells peaked at 30 min and declined over 2 h (Figure 3A), while the amount of RF confined to the mitochondria increased over time in Caco-2 cells (data not shown). Despite this divergent accumulation profile in the two cell models, the maximal mitochondrial RF content was no greater than 30% of the postnuclear load, whereas TF levels associated with the mitochondria were negligible in comparison (Figure 3B).

To further corroborate the Golgi and mitochondrial fate of RF, 3D colocalization of Rd−RF and FITC−TF by confocal microscopy together with the same organelle markers (i.e., GM130 and cytochrome *c*) was assessed. Both ligands were shown to colocalize to some degree with these organelle markers (Figure 7B,D). As noted with the endocytic proteins, Rd−RF and FITC−TF resulted in punctate and perinuclear colocalization with GM130 and cytochrome *c*. Image analyses for both ligands revealed a positive Pearson's correlation with GM130 and cytochrome *c*, thus further suggesting the involvement of these organelles in RF and TF trafficking. Rd−RF exhibited a higher degree of colocalization (∼34%) with GM130 (Figure 6A) that was approximately 2-fold higher than that determined for FITC−TF (Figure 6B). FITC−TF also revealed the smallest amount of colocalization (∼8%) with the mitochondrial marker, cytochrome *c* (Figure 6B). In contrast, Rd−RF revealed greater than 3-fold higher overlap (∼26%) with cytochrome *c* (Figure 6A). On the basis of the current understanding of RF physiology and the role of its cofactors, FMN and FAD, in metabolic functioning of the cell, the distribution to the mitochondria appears to be consistent.

cAMP Regulation of RF Binding and Initiation of the Endocytic Cascade. Cyclic AMP is unequivocally a major short-term regulator that regulates autologous or heterologous receptor-mediated endocytic internalization (*37*). Previous reports have shown that increased levels of cAMP elicited by forskolin, Br-cAMP, and 3-isobutyl-1-methylxanthine (IBMX) have resulted in a dramatic reduction in the rate of RF uptake in BeWo cells (*4*, *5*). In the study presented here, the role of cAMP was evaluated at the principal step of ligand recognition and binding by the RF-specific plasma membrane-associated receptors. BeWo cells stimulated with increasing concentrations of forskolin resulted in a robust cAMP response with an EC_{50} of 1.5 μM (0.99−1.9) and a B_{max} value of 125 ± 2.2 pmol of cAMP/250 000 cells, while treatment with riboflavin up to 10^{-4} M failed to stimulate any cAMP accumulation (Figure 8A). Interestingly, pretreatment of BeWo cells with increasing concentrations of RF for merely 10 min prior to stimulation with 1 μM forskolin in the continued presence of RF resulted in a weakened cAMP response (Figure 8B). The maximum inhibition was ∼67% of control with a reported IC_{50} value of ∼0.4 μM. This indicates that RF bound to the putative RF receptor is negatively coupled to cAMP and suggests that stimulated cAMP production consequently results in a decreased rate of uptake via clathrin-coated pits.

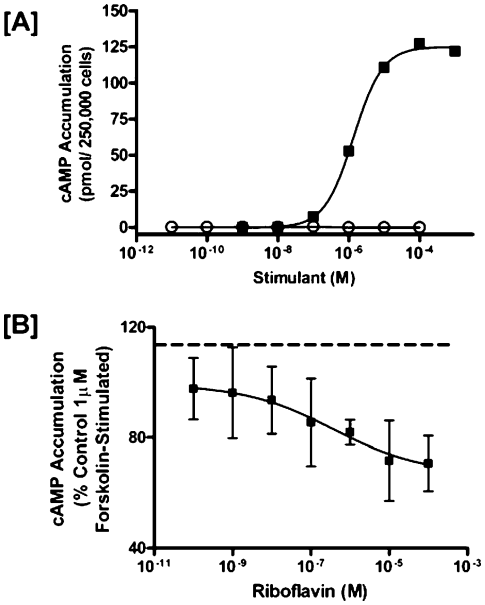

FIGURE 8: Cyclic AMP regulation of the RF internalization process. (A) Determination of cAMP accumulation in BeWo cells after stimulation with riboflavin or forskolin. BeWo cells cultured as described in Experimental Procedures were stimulated via incubation with the indicated concentration of either forskolin (■) for 10 min or riboflavin (○) for 40 min. Data give a representative curve from three independent experiments showing similar results. (B) Inhibitory effects of riboflavin on forskolin-stimulated cAMP accumulation. BeWo cells were washed and then incubated with the indicated concentrations of riboflavin dissolved in HF12K (20 mM HEPES-buffered F12K at pH 7.4 and 37 °C). After 10 min, HF12K was removed and cells were stimulated with 1 μM forskolin in the continued presence of riboflavin. cAMP accumulation was then assessed as described in Experimental Procedures. The dashed line indicates 1 μM forskolin stimulated accumulation in the absence of riboflavin. Results are expressed as the mean ± the standard deviation ($n = 5$).

DISCUSSION

Our laboratory has recently demonstrated that intestinal and placental entry of vitamin B_2 into the cell occurs via a putative receptor-mediated endocytic process (*3*, *4*, *19*). This RF-specific endocytic pathway is still in its nascent stage of identification and has warranted investigative pursuits to clearly define its translocation pathway within the cell. In this study, we delineate the trafficking route of RF upon internalization that consequently contributes to the maintenance of vitamin homeostasis. In addition, we report second-messenger regulation of the ligand absorption into placental trophoblasts that suggests interaction of other extrinsic pathways in response to the ligand stimulus.

The approach that was employed followed a conventional fractionation analysis of intracellular compartments that are integral to the "classical" clathrin-dependent endocytic machinery. The BeWo cell line exhibited distinctive accumulations for RF and TF within the endocytic system but negligible levels for a nonendocytic marker TCA, which is routinely transported by placental bile acid transporters (*38*). Sucrose density gradient-resolved endosomal and lysosomal fractions defined by widely used organelle markers (clathrin, Rab5 GTPase, and LAMP-1) showed extensive labeling for RF and TF within the endosomes. Selective enrichment of the endosomes over lysosomes for both ligands was in accordance with previously determined trafficking profiles for TF (*29*−*31*) and confirmed the efficiency of the

fractionation method. The method also provided insight into the possible fate of RF following internalization. Biochemical association with the mitochondrial compartment is expected since FMN and FAD play a pivotal role in the electron transport chain (*39*), generating the metabolic energy required for other cellular functions.

Trophoblasts exhibited comparatively higher uptake levels for TF than RF. This may be attributed to the differential nutritional needs of the cell for iron and vitamin B_2. van der Ende and colleagues (*40*) have demonstrated that the augmented process of iron transfer and metabolism in the developing fetus is efficiently mediated by the transplacental TF system. Likewise, gestational needs of RF are also increased (*2*), and a subsequent increase in the RF supply would be expected. Further, a time-associated increase in ligand buildup was observed for RF and TF within the endocytic compartments. The endocytic process entails rapid internalization of recognized ligands; consequently, evaluation of time points shorter than 30 min is currently underway using real-time confocal microscopy. Nevertheless, this method provides an informative overview of the trafficking itinerary of RF via the endocytic route. The kinetic distribution of 5−25 nM RF expectedly showed an increased level of accumulation within the organelles examined with the exception of mitochondrial compartments. Clearly, the changing distribution patterns of RF within the mitochondria suggest a tightly regulated feedback mechanism that controls the trafficking route of the molecule, which in turn maintains a homeostatic check on the cellular RF content. It is very likely that the increased level of RF accumulation over time provides the impetus for rapidly converting RF to the flavin intermediates that cycle through the metabolic pathway. This dynamic change in compartmentalized RF presents a challenging scenario of putative RF sensors, receptors, and other regulators that must interact to maintain a balanced nutritional environment.

A limitation of any fractionation method is the potential overlap between the organelles that have been identified. Consequently, to further corroborate the intracellular distribution profiles of RF, a minimally invasive labeling approach examining the colocalization of fluorescently labeled ligands with immunostained organelle markers was utilized. The pattern of rhodamine-conjugated riboflavin, a derivative of the natural ligand previously characterized in our laboratory (*18*) that retains affinity for the RF transport system, was compared with the staining patterns of FITC−TF. Rd−RF convincingly localized within the endosomes, lysosomes, Golgi, and mitochondria, whereas FITC−TF was confined predominantly to the endosomes. It is not clear at this time what the significance of localization to the Golgi may signify, but this may reflect a possible recycling mechanism that recovers RF and packages it for either storage or exocytosis. Evidence for Golgi processing of the TF receptor is seen in myeloma cells and supports the recycling theory of this receptor that continuously scavenges iron-bound TF (*41*). In fact, prior studies reveal two types of recycling pathways, i.e., a short pathway involving early endosomal fusion with recycling endosomes that target ligands back to the plasma membrane and a long pathway that translocates ligands to the Golgi, at which clathrin initiates vesicular budding from the trans-most cisternae and eventual shuttling to the plasma membrane (*10*, *42*, *43*). A recycling component specific to the RF trafficking itinerary has yet to be defined; however, it would be interesting to delineate whether one or both of these recycling events are specific to this vitamin. It should be noted that the possibility of equilibrative changes associated with time-resolved imaging cannot be ruled out at this juncture, and identification of such events requires real-time imaging approaches. However, the intent of this study was to illustrate the involvement of the endocytic machinery in the cellular trafficking itinerary of RF.

The presence of a receptor-mediated endocytic component in the placental internalization of RF then raises several questions regarding its effectors and regulators that need to be addressed. Literature reports have established that the endocytic process in eukaryotes occurs through a highly ordered process and is driven by signaling events that activate or inactivate depending upon the stimulus (*37*). Cyclic AMP is clearly a pivotal candidate integral to a large number of signaling cascades and was evaluated as a key regulator of the RF endocytic process. RF alone did not generate a cAMP response, but it was responsible for downregulating the cAMP production upon stimulation with forskolin. This indicates that the ligand-sequestered RF receptor lowers the intracellular levels of cAMP prior to its association into clathrin-coated pits and eventually triggers the subsequent endocytic events of sorting and translocation. Conversely, we have already shown that increased stores of intracellular cAMP significantly inhibit the internalization of RF (*4*), thereby indicating an inverse relationship between intracellular cAMP and RF receptor-mediated endocytosis.

In conclusion, fractionation data taken together with the morphological assessment of cellular RF distribution provide definitive evidence of endocytic trafficking of RF, at least in part via a clathrin-dependent pathway, and eventual translocation to the mitochondria where the role of its metabolites is well-characterized. In addition, this cellular absorption mechanism is shown to be sensitive to cAMP levels, further suggesting the existence of a highly regulated RF-specific receptor internalization process. Understanding the characteristics of the RF translocation pathway provides a novel platform that can be potentially exploited in the future, analogous to the folate and transferrin receptors in biomedical imaging (*44*) and tumor-targeted delivery of genes or therapeutic conjugates (*45*−*48*).

ACKNOWLEDGMENT

We acknowledge confocal and imaging specialists Chris Cathcart, Jesse Dewitt, and Marc Benvenuto (Nikon Image Systems, Inc., Columbia, MD) for their technical expertise with the confocal microscopy studies. We also thank Dr. Robert J. Bloch (Department of Physiology, University of Maryland, Baltimore, MD) for important suggestions and review of the manuscript and Dr. Mitch A. Phelps (The Ohio State University, Columbus, OH) for valuable discussions throughout the study.

REFERENCES

1. Cooperman, J. M., and Lopez, R. (1991) Riboflavin, in *Handbook of vitamins*, pp 283−310, Marcel Dekker, New York.
2. Powers, H. J. (2003) Riboflavin (vitamin B-2) and health, *Am. J. Clin. Nutr. 77*, 1352−60.
3. Huang, S. N., and Swaan, P. W. (2000) Involvement of a receptor-mediated component in cellular translocation of riboflavin, *J. Pharmacol. Exp. Ther. 294*, 117−25.

4. Huang, S. N., and Swaan, P. W. (2001) Riboflavin uptake in human trophoblast-derived BeWo cell monolayers: Cellular translocation and regulatory mechanisms, *J. Pharmacol. Exp. Ther. 298*, 264−71.
5. Foraker, A. B., Khantwal, C. M., and Swaan, P. W. (2003) Current perspectives on the cellular uptake and trafficking of riboflavin, *Adv. Drug Delivery Rev. 55*, 1467−83.
6. Mason, C. W., D'Souza, V. M., Bareford, L. M., Phelps, M. A., Ray, A., and Swaan, P. W. (2006) Recognition, Co-internalization and Recycling of an Avian Riboflavin Carrier Protein in Human Placental Trophoblasts, *J. Pharmacol. Exp. Ther.* (in press).
7. Holladay, S. R., Yang, Z., Kennedy, M. D., Leamon, C. P., Lee, R. J., Jayamani, M., Mason, T., and Low, P. S. (1999) Riboflavin-mediated delivery of a macromolecule into cultured human cells, *Biochim. Biophys. Acta 1426*, 195−204.
8. Wangensteen, O. D., Bartlett, M. M., James, J. K., Yang, Z. F., and Low, P. S. (1996) Riboflavin-enhanced transport of serum albumin across the distal pulmonary epithelium, *Pharm. Res. 13*, 1861−4.
9. Aw, T. Y., Jones, D. P., and McCormick, D. B. (1983) Uptake of riboflavin by isolated rat liver cells, *J. Nutr. 113*, 1249−54.
10. Maxfield, F. R., and McGraw, T. E. (2004) Endocytic recycling, *Nat. Rev. Mol. Cell Biol. 5*, 121−32.
11. Barbieri, M. A., Ramkumar, T. P., Fernadez-Pol, S., Chen, P. I., and Stahl, P. D. (2004) Receptor tyrosine kinase signaling and trafficking: Paradigms revisited, *Curr. Top. Microbiol. Immunol. 286*, 1−20.
12. Schulte, G., and Fredholm, B. B. (2003) The G(s)-coupled adenosine A(2B) receptor recruits divergent pathways to regulate ERK1/2 and p38, *Exp. Cell Res. 290*, 168−76.
13. Pattillo, R. A., and Gey, G. O. (1968) The establishment of a cell line of human hormone-synthesizing trophoblastic cells in vitro, *Cancer Res. 28*, 1231−6.
14. Dancis, J., Lehanka, J., and Levitz, M. (1988) Placental transport of riboflavin: Differential rates of uptake at the maternal and fetal surfaces of the perfused human placenta, *Am. J. Obstet. Gynecol. 158*, 204−10.
15. Kirshenbaum, N. W., Dancis, J., Levitz, M., Lehanka, J., and Young, B. K. (1987) Riboflavin concentration in maternal and cord blood in human pregnancy, *Am. J. Obstet. Gynecol. 157*, 748−52.
16. Visweswariah, S. S., and Adiga, P. R. (1987) Isolation of riboflavin carrier proteins from pregnant human and umbilical cord serum: Similarities with chicken egg riboflavin carrier protein, *Biosci. Rep. 7*, 563−71.
17. Dancis, J., Lehanka, J., and Levitz, M. (1985) Transfer of riboflavin by the perfused human placenta, *Pediatr. Res. 19*, 1143−6.
18. Phelps, M. A., Foraker, A. B., Gao, W., Dalton, J. T., and Swaan, P. W. (2004) A novel rhodamine-riboflavin conjugate probe exhibits distinct fluorescence resonance energy transfer that enables riboflavin trafficking and subcellular localization study, *Mol. Pharm. 1*, 257−66.
19. Huang, S. N., Phelps, M. A., and Swaan, P. W. (2003) Involvement of endocytic organelles in the subcellular trafficking and localization of riboflavin, *J. Pharmacol. Exp. Ther. 306*, 681−7.
20. Dautry-Varsat, A., Ciechanover, A., and Lodish, H. F. (1983) pH and the recycling of transferrin during receptor-mediated endocytosis, *Proc. Natl. Acad. Sci. U.S.A. 80*, 2258−62.
21. van Dam, E. M., and Stoorvogel, W. (2002) Dynamin-dependent transferrin receptor recycling by endosome-derived clathrin-coated vesicles, *Mol. Biol. Cell 13*, 169−82.
22. Jin, M., and Snider, M. D. (1993) Role of microtubules in transferrin receptor transport from the cell surface to endosomes and the Golgi complex, *J. Biol. Chem. 268*, 18390−7.
23. Zhang, E. Y., Phelps, M. A., Banerjee, A., Khantwal, C. M., Chang, C., Helsper, F., and Swaan, P. W. (2004) Topology scanning and putative three-dimensional structure of the extracellular binding domains of the apical sodium-dependent bile acid transporter (SLC10A2), *Biochemistry 43*, 11380−92.
24. Zhang, E. Y., Knipp, G. T., Ekins, S., and Swaan, P. W. (2002) Structural biology and function of solute transporters: Implications for identifying and designing substrates, *Drug Metab. Rev. 34*, 709−50.
25. Manders, M. M., Verbeek, P. J., and Aten, J. A. (1993) Measurement of co-localization of objects in dual colour confocal images, *J. Microsc. (Oxford, U.K.) 169*, 375−82.
26. Nathke, I. S., Heuser, J., Lupas, A., Stock, J., Turck, C. W., and Brodsky, F. M. (1992) Folding and trimerization of clathrin subunits at the triskelion hub, *Cell 68*, 899−910.
27. Bucci, C., Parton, R. G., Mather, I. H., Stunnenberg, H., Simons, K., Hoflack, B., and Zerial, M. (1992) The small GTPase rab5 functions as a regulatory factor in the early endocytic pathway, *Cell 70*, 715−28.
28. Rohrer, J., Schweizer, A., Russell, D., and Kornfeld, S. (1996) The targeting of Lamp1 to lysosomes is dependent on the spacing of its cytoplasmic tail tyrosine sorting motif relative to the membrane, *J. Cell Biol. 132*, 565−76.
29. Yamashiro, D. J., and Maxfield, F. R. (1984) Acidification of endocytic compartments and the intracellular pathways of ligands and receptors, *J. Cell. Biochem. 26*, 231−46.
30. Ciechanover, A., Schwartz, A. L., Dautry-Varsat, A., and Lodish, H. F. (1983) Kinetics of internalization and recycling of transferrin and the transferrin receptor in a human hepatoma cell line. Effect of lysosomotropic agents, *J. Biol. Chem. 258*, 9681−9.
31. Yamashiro, D. J., Tycko, B., Fluss, S. R., and Maxfield, F. R. (1984) Segregation of transferrin to a mildly acidic (pH 6.5) para-Golgi compartment in the recycling pathway, *Cell 37*, 789−800.
32. McLauchlan, H., Newell, J., Morrice, N., Osborne, A., West, M., and Smythe, E. (1998) A novel role for Rab5-GDI in ligand sequestration into clathrin-coated pits, *Curr. Biol. 8*, 34−45.
33. Gorvel, J. P., Chavrier, P., Zerial, M., and Gruenberg, J. (1991) rab5 controls early endosome fusion in vitro, *Cell 64*, 915−25.
34. Jackle, S., Runquist, E. A., Miranda-Brady, S., and Havel, R. J. (1991) Trafficking of the epidermal growth factor receptor and transferrin in three hepatocytic endosomal fractions, *J. Biol. Chem. 266*, 1396−402.
35. Nakamura, N., Rabouille, C., Watson, R., Nilsson, T., Hui, N., Slusarewicz, P., Kreis, T. E., and Warren, G. (1995) Characterization of a cis-Golgi matrix protein, GM130, *J. Cell Biol. 131*, 1715−26.
36. Gonzales, D. H., and Neupert, W. (1990) Biogenesis of mitochondrial c-type cytochromes, *J. Bioenerg. Biomembr. 22*, 753−68.
37. Foti, M., Carpentier, J. L., Aiken, C., Trono, D., Lew, D. P., and Krause, K. H. (1997) Second-messenger regulation of receptor association with clathrin-coated pits: A novel and selective mechanism in the control of CD4 endocytosis, *Mol. Biol. Cell 8*, 1377−89.
38. Dumaswala, R., Setchell, K. D., Moyer, M. S., and Suchy, F. J. (1993) An anion exchanger mediates bile acid transport across the placental microvillous membrane, *Am. J. Physiol. 264*, G1016−23.
39. Barile, M., Brizio, C., Valenti, D., De Virgilio, C., and Passarella, S. (2000) The riboflavin/FAD cycle in rat liver mitochondria, *Eur. J. Biochem. 267*, 4888−900.
40. van der Ende, A., du Maine, A., Simmons, C. F., Schwartz, A. L., and Strous, G. J. (1987) Iron metabolism in BeWo chorion carcinoma cells. Transferrin-mediated uptake and release of iron, *J. Biol. Chem. 262*, 8910−6.
41. Woods, J. W., Doriaux, M., and Farquhar, M. G. (1986) Transferrin receptors recycle to cis and middle as well as trans Golgi cisternae in Ig-secreting myeloma cells, *J. Cell Biol. 103*, 277−86.
42. Ghosh, R. N., and Maxfield, F. R. (1995) Evidence for nonvectorial, retrograde transferrin trafficking in the early endosomes of HEp2 cells, *J. Cell Biol. 128*, 549−61.
43. Sakai, T., Mizuno, T., Miyamoto, H., and Kawasaki, K. (1998) Two distinct kinds of tubular organelles involved in the rapid recycling and slow processing of endocytosed transferrin, *Biochem. Biophys. Res. Commun. 242*, 151−7.
44. Berry, C. C., Charles, S., Wells, S., Dalby, M. J., and Curtis, A. S. (2004) The influence of transferrin stabilised magnetic nanoparticles on human dermal fibroblasts in culture, *Int. J. Pharm. 269*, 211−25.
45. Yoo, H. S., and Park, T. G. (2004) Folate-receptor-targeted delivery of doxorubicin nano-aggregates stabilized by doxorubicin-PEG-folate conjugate, *J. Controlled Release 100*, 247−56.
46. Yoo, H. S., and Park, T. G. (2004) Folate receptor targeted biodegradable polymeric doxorubicin micelles, *J. Controlled Release 96*, 273−83.
47. Li, Y., Ogris, M., Wagner, E., Pelisek, J., and Ruffer, M. (2003) Nanoparticles bearing polyethylene glycol-coupled transferrin as gene carriers: Preparation and in vitro evaluation, *Int. J. Pharm. 259*, 93−101.
48. Hattori, Y., and Maitani, Y. (2004) Enhanced in vitro DNA transfection efficiency by novel folate-linked nanoparticles in human prostate cancer and oral cancer, *J. Controlled Release 97*, 173−83.

BI060138F